Continental Shelf Research 259 (2023) 104984

Contents lists available at ScienceDirect

Continental Shelf Research

journal homepage: www.elsevier.com/locate/csr

Research papers

An inventory of salty and warm subsurface intrusions in the South Brazil Bight

Danilo Augusto Silva [a,*], Dalton Kei Sasaki [a], Marcelo Dottori [a], Ilson Carlos Almeida da Silveira [a], Wellington Ceccopieri Belo [b], Renato Parkinson Martins [b]

[a] Oceanographic Institute, University of Sao Paulo, Praca do Oceanografico, 191, SP 05508-120, São Paulo, Brazil
[b] Centro de Pesquisas, Desenvolvimento e Inovação Leopoldo Américo Miguez de Mello - CENPES/PETROBRAS, Av. Horácio Macedo, 950 - Cidade Universitária da Universidade Federal do Rio de Janeiro, Rio de Janeiro - RJ, 21941-915, Brazil

ARTICLE INFO

Keywords:
Salty warm intrusions
Brazil current
Cross-shelf exchange

ABSTRACT

Subsurface intrusions of salty and warm waters onto the shelf can potentially impact the thermodynamics and biogeochemistry of these relatively shallow water environments. Such thermohaline intrusions are usually associated with double diffusive processes and can enhance the vertical and lateral fluxes. In this work, we characterized subsurface intrusions of Tropical Waters (TW) at the South Brazil Bight (SBB) - a mid-latitude continental shelf, which were detected based on salinity vertical profiles from a historical dataset. We found the intrusions tend to follow the pycnocline and are relatively common year-round, occurring at 27% of the dataset, with a maximum salinity highly correlated with the maximum stratification. Intrusions have different along-shelf characteristics, varying with the shelf width and depth. North of São Sebastião Island (SSI) – at the central portion of the SBB –, intrusions were thicker, saltier, and shallower than the ones found at the south of SSI. These differences could be related to the variations of the Coastal Water (CW) and South Atlantic Central Water (SACW) volume along the shelf and throughout the year. We found that intrusions' thickness presents an inverse correlation with stratification, resulting in thinner intrusions in more stratified environments. This inverse correlation suggests double-diffusively driven intrusions. We apply the Turner Angle method to investigate whether the environment is susceptible to double diffusive processes. This analysis suggests that thermohaline intrusions in the SBB might not be primarily double diffusive. However, the dominance of different double diffusion processes - diffusive convection (salt fingering) at the upper (lower) layer - suggests that these processes influence intrusion growth, steady-state, and erosion. Nonetheless, the mechanism responsible for the initial density perturbation remains unknown and further studies are needed to explore the relationship between the Brazil Current dynamics and thermohaline warm and salty subsurface intrusions.

1. Introduction

All over the world, interleaving layers of different water masses with similar densities are found in frontal zones (Roden, 1964; Beal, 2007), whether in deep or coastal regions (Ruddick and Richards, 2003). These features, often called thermohaline intrusions, have vertical scales of O(10–100 m) and horizontal scales of O(1–100 km) (Stommel and Fedorov, 2016; Joyce et al., 1978; Perkin and Lewis, 1984; Ruddick and Hebert, 1988). For instance, in the Middle Atlantic Bight, interleaving layers are detected by intrusions of anomalously salty water and occur commonly across the outer shelf at the depth of the seasonal pycnocline (Lentz, 2003).

Intrusions are attributed to strong lateral fluxes and enhanced vertical gradients (Ruddick and Hebert, 1988; Ruddick and Richards, 2003). They also impact air-sea interactions (Boyd and D'Asaro, 1994) and larvae exchange between shelf and shelf-slope (Wang and Jordi, 2011; Namiki et al., 2017). Thus, they can potentially affect the local thermodynamics, the biogeochemistry of the shelf (Woods et al., 1986; Ruiz-Castillo et al., 2019), and even influence the global climate (Robertson et al., 1995).

Thermohaline intrusions are typically formed from a finite disturbance in the density structure of a frontal zone (Jan et al., 2019), which can be triggered by several processes, like cross-shelf horizontal density gradient (Welch, 1981), internal waves (Hopkins et al., 2012), wind stress (González-Pola et al., 2007; Ruiz-Castillo et al., 2019) and mesoscale activity (Li et al., 2012; Malan et al., 2020), just to name

* Corresponding author.
E-mail address: danilo2.silva@usp.br (D.A. Silva).

https://doi.org/10.1016/j.csr.2023.104984
Received 10 June 2022; Received in revised form 20 February 2023; Accepted 29 March 2023
Available online 31 March 2023

a few. The intrusion growth is driven either by advective processes, differential diffusion of heat and salt, or by both (May and Kelley, 1997). The former process is related to the baroclinicity (Kuzmina and Rodionov, 1992; May and Kelley, 1997, 2002), while the latter is related to double-diffusion processes (Stern, 1967; Ruddick and Turner, 1979; Toole and Georgi, 1981) in its two forms: salt fingering and diffusive convection.

At the southwestern South Atlantic, intrusions were observed in the Brazil-Malvinas Confluence (BMC) and the Argentinean Basin (Georgi, 1981; Piola and Georgi, 1982; Bianchi et al., 1993; Provost et al., 1995). In this region, intrusive structures were found to last approximately one week (Bianchi et al., 1993), due to a large intrusive fluxes (Provost et al., 1995; Ruddick and Richards, 2003) that will dissipate small intrusions (Bianchi et al., 1993). At the South Brazil Bight (SBB), a tongue-shaped pattern of salty and warm waters penetrating the inner area of the continental shelf (see Figure 6 in Campos et al., 2000) was found in observational datasets (de Castro, 1996; Campos et al., 2000; Castro, 2014) and in numerical outputs (Palma and Matano, 2009) on this shelf. During summer and winter, lanternfish larvae, dominant in the larval oceanic assemblages (Olivar and Shelton, 1993; Muhling et al., 2008; Katsuragawa et al., 2014), were found within the inner and mid-shelves of the SBB (Namiki et al., 2017). The authors associated their occurrence with TW intrusions throughout the year, mostly due to the Brazil Current mesoscale activity.

Although these intrusions had been presented in other studies, no special attention has been given to their characteristics, like the frequency of occurrence, vertical position of the intrusive core or salinity anomaly associated with these features. In this study, we address the occurrence of TW subsurface thermohaline intrusions in the SBB, exploring their median properties, distribution along the shelf, and its implications for thermohaline motion.

This article is structured as follows: Section 2 provides an overview of the study area, in Section 3 we present the historical dataset used to identify intrusions at the SBB. The detection algorithm is described in Section 4, along with statistical and descriptive analysis. Section 5 presents a descriptive characterization of the intrusions, while Section 6 investigates the underlying thermohaline processes. We conclude this work with a discussion in Section 7.

2. The south BrazilBight (SBB)

The South Brazil Bight (SBB) is a mid-latitude continental shelf, located in the southwestern South Atlantic. It presents a variable width ranging from, approximately, 70 km, in its extremities, to about 230 km in its central part (Castro, 2014). The freshwater input is mainly related to small river runoff along the coast (Castro and Miranda, 1998) that generate a low salinity line source nearshore (de Castro, 1996). Among the rivers, the Ribeira de Iguape River discharge - located in Cananéia (Fig. 1) - accounts for 60% of the total discharge at the SBB (Marta-Almeida et al., 2021). Moreover, in ideal conditions, the La Plata river plume can reach the SBB, affecting the temperature and salinity of the inner portion of the shelf specially during the winter (Piola, 2005).

The outflow of small rivers along the coast, combined with the synoptic wind regime, dominates the inner shelf circulation (de Castro, 1996; Castro, 2014), resulting in northeastward flow (Fontes and de Castro, 2017). The middle shelf has a barotropic response to the wind regime, with the direction depending on that of the wind, both local (Dottori and Castro, 2009) and remote (Dottori and Castro, 2018). The outer shelf circulation is primarily driven by the Brazil Current (BC) and, to a weaker degree, by the synoptic wind (Castro et al., 2008). The BC flows southwestward along the continental slope. Eventually, part of its transport reaches the SBB across the shelf break (da Silveira et al., 2000).

The BC transports, within its mixed layer, the Tropical Water (TW), which is a warmer and saltier ($T > 21$ °C, $S > 36.4$ g kg^{-1}) water (Miranda, 1982), and below its pycnocline, the BC transports the South Atlantic Central Water (SACW), with waters relatively colder and fresher ($T < 18$ °C, $S < 36$ g kg^{-1}) (Miranda, 1982). The eventual transport of these two oceanic waters reaches the shelf and the mixing between them with continental runoff results in a third water mass, the Coastal Water (CW), characterized by the lowest salinity values among the three water masses (Castro and Miranda, 1998). At the surface, a steep salinity gradient forms the Surface Haline Front (SHF) and the isohaline of 36 PSU defines the inshore limit of influence of the TW (Castro, 2014). Below the surface, the transition between the TW and the SACW forms the thermocline, which eventually reaches the bottom.

The São Sebastião Island (SSI; Fig. 1), located near the central portion of the SBB, acts as a boundary between two distinct environments at the SBB. To the south of SSI, the continental shelf has its widest width (~230 km) and a smooth bathymetry, with the freshwater contribution of the Ribeira de Iguape River (Marta-Almeida et al., 2021) and the Santos-São Vicente-Bertioga estuarine system (de Castro, 1996). However, to the north, the shelf is narrower (~50 km) which implies that oceanic waters flow relatively closer to the coast (Mahiques et al., 2004). In addition, the northern area of the SBB does not have a larger influence of river runoff and, during summer and autumn (Cerda and Castro, 2014; Castro, 2014), the region presents its lowest salinity in the vicinity of Ubatuba, due to the horizontal advection of low salinity waters from south of SSI (Castro, 2014). The different conditions in which north and south are susceptible also results in different hydrographics conditions, with a south dominated by CW and SACW and TW dominating the northern part (Dottori et al., 2023).

The TW, eventually, moves towards the coast at subsurface levels. During intrusive events, a salinity maximum was found at a depth of approximately 50 m (Campos et al., 2000; Castro, 2014) in observational datasets during winter in the central portion of the SBB. A regional climatology of the area shows a signal of shoreward TW advection at 25 m throughout the year, between the SSI and Cabo Frio (Cerda and Castro, 2014). In addition, Palma and Matano (2009) reproduced, numerically, a similar intrusive structure at the region in winter, with maximum salinity found at 50 m (see their Fig. 4). A common feature among all these cases is the presence of CW above the intrusive layer and, in some events, the SACW was found below the intrusion.

3. Historical dataset

The intrusion characterization was made by using an extensive historical dataset available at the Coastal Hydrodynamics Laboratory from the Oceanographic Institute of the University of São Paulo, and at the National Oceanographic Database (NOD or, in Brazilian Portuguese, BNDO), maintained by the Brazilian Navy. This dataset comprises approximately 14 projects carried out in the region since the 1980s, using water bottles and CTD. In addition, we used hydrographic vertical profiles, from the Santos Project – Santos Basin Environmental Characterization – coordinated by PETROBRAS, in collaboration with the Oceanographic Institute of the University of São Paulo. Table 1 summarizes the projects and the period of sampling used in this work. The density of observations resulting from this collection of data is exemplified in Fig. 1, totalizing 2160 vertical profiles from CTD and bottle samples within the continental shelf. Since we are interested in intrusions at the inner and mid-shelf, we select casts between the coast and the 110-m isobath. This was a choice based on the TW location, which is usually restricted to the mid-shelf (Castro, 2014).

The collection of data was pre-processed rigorously, using Python–CTD (Fernandes, 2014). Only vertical profiles with at least 5 consecutive measurements and with a maximum vertical distance of 25 m apart were considered. This filtering process is similar to the one applied by Lentz (2003) and by Castelao (2011) to select historical data in their studies. Exclusively for the CTD casts, spikes were removed considering a 4 standard deviation threshold from the average. The data was then binned to every meter and smoothed with a 7–point window Hanning

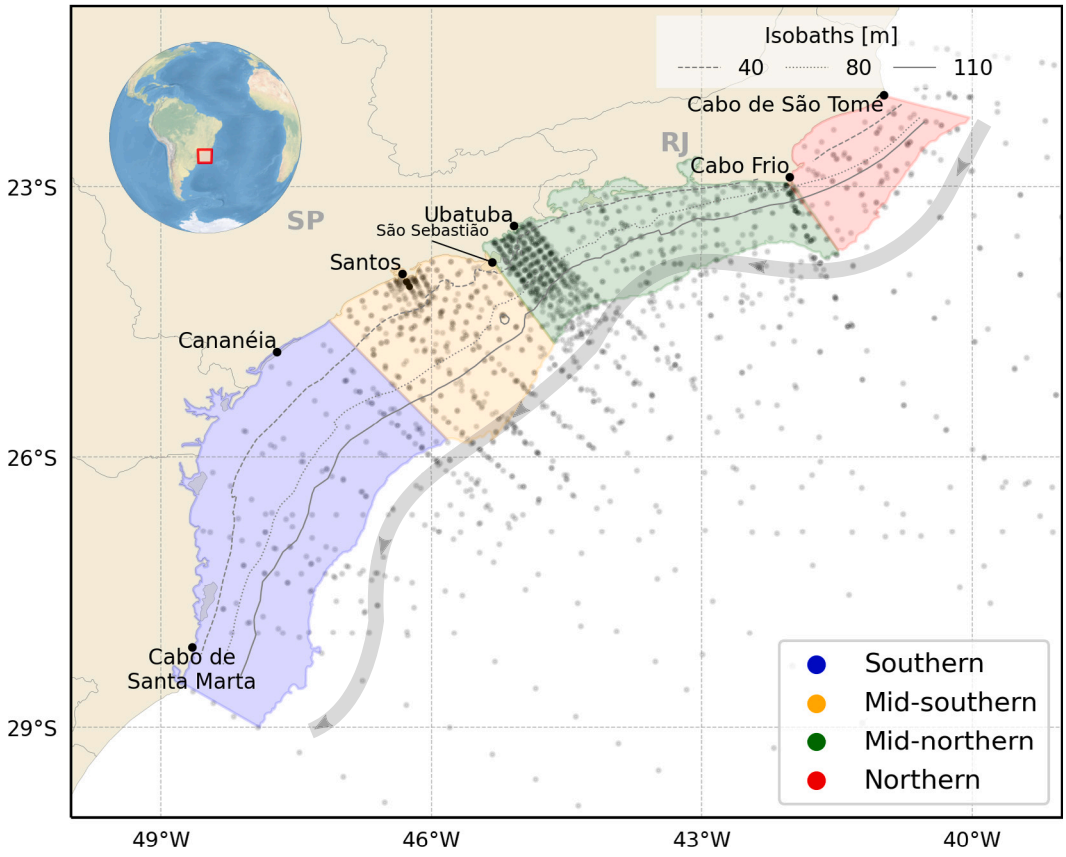

Fig. 1. Study area map covering the main limits of the South Brazil Bight continental shelf, from Santa Marta Cape, at south, to São Tomé Cape, at north. Gray dots represent the historical dataset sampling distribution and lines are the 40-, 80-, and 110-m isobaths. The shaded colored regions represent the compartmentalization created in this work, to evaluate the intrusion distribution and properties along shelf. Each compartment is bounded offshore by the 200-m isobath. The red thicker line represents the Brazil Current average position.

Table 1
Summary of all projects used, the number of casts considered and the period of observation.

Project	Profiles[a]	Period[b]
PIOF	452	12/1985 – 07/1988[c]
COROAS	294	01/1993 – 01/1994
Oceano Sudeste	384	05/2000 – 11/2006
DEPROAS	138	02/2001 – 07/2002
CARMIN	288	05 – 08/2001
ECOSAN	264	09/2005 – 03/2006
NOD/BNDO	176	01/1996 – 10/2016[d]
SANAGU	60	08 – 10/2019
SANSED	104	06 – 11/2019

[a]Only considered vertical profiles between the coastline and the 110 m isobath, which were used in the detection algorithm.
[b]Estimated period, with sampling performed in a few months between the initial and final date.
[c]PIOF sampling was performed during December from 1985 to 1987 and during July from 1986 to 1988.
[d]NOD is a data collection and the period shown is based on the first and last projects used in this work.

filter. Due to discrepancies in sample distributions along the shelf (Fig. 1), we divided the SBB into four regions based on relevant features of the area. The Southern (S) compartment is delimited between the Cabo de Santa Marta and approximately 24 °S, based on the maximum extension of the La Plata River plume (Piola, 2005). The Mid-Southern (MS) boundary is based on the climatological influence of the inner shelf northeastward currents due to buoyancy forcing (Castro, 2014), and it is defined as the region between 24 °S and São Sebastião Island (SSI). The Mid-Northern (MN) region is established between São Sebastião Island and Cabo Frio, where the coastline changes its orientation from E-W to N-S. Finally, the Northern (N) region goes from Cabo Frio to Cabo de São Tomé, the northern border of the SBB (Castro and Miranda, 1998). The compartments are shown in Fig. 1.

4. Methods

4.1. Algorithm detection

The occurrence of subsurface intrusions in the South Brazil Bight was investigated with the algorithm proposed by Lentz (2003) with adaptations to the SBB region. The algorithm identifies subsurface intrusions in salinity vertical profiles (from CTD or bottle samples) based on the vertical finite difference between consecutive samples, detecting an intrusion when the vertical gradient reaches a specific threshold, determined by a salinity difference (dS).

This algorithm was used to identify subsurface intrusions in historical vertical profiles in the Middle Atlantic Bight (MAB), considering a salinity threshold of dS = 0.1 g kg^{-1} m^{-1} (Lentz, 2003). In this study, we identified the same threshold as the best choice for the SBB, based on sensitive tests for several values. However, we considered an increase of dS with depth, instead of a decrease as in the original algorithm. This change is only possible because in the SBB, salinity increases with depth at the upper layers, differently from the region where Lentz (2003) applied his algorithm.

Usually, it is possible to identify TW based solely on a salinity value of 36.4 g kg^{-1}. However, the algorithm did not identify significant

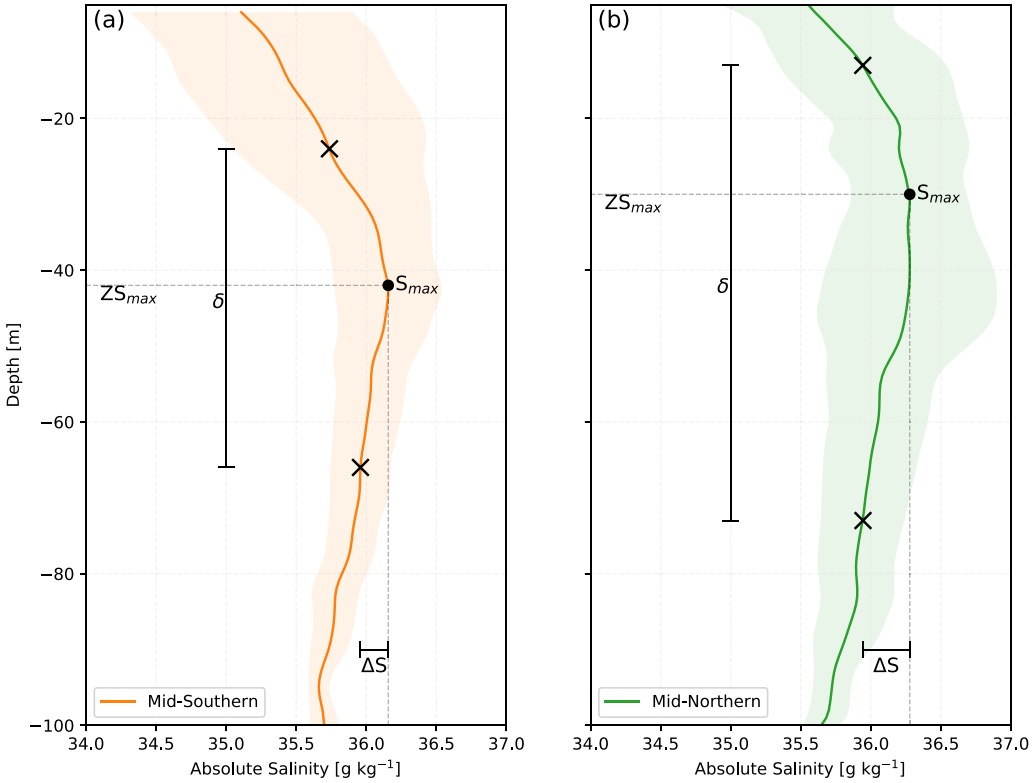

Fig. 2. Average absolute salinity vertical profile and envelope of observations with subsurface thermohaline intrusion, constructed from the historical observational dataset identified with intrusion by the algorithm applied in this work. (a) shows the typical conditions from the region south of São Sebastião Island, while (b) is for the north region. Check Fig. 3 for a geographical location.

intrusive events in the dataset. The TS diagrams for the SBB show that salinity of 36 g kg^{-1} is an appropriate value to identify the SACW/TW interface. The adjustment for the algorithm to identify intrusions with maximum salinity higher than these values increased the algorithm's performance. Since we are interested in subsurface intrusions of Tropical Waters (TW), we restrict the algorithm to find maximum salinities higher than 36 g kg^{-1} (in these cases, TW dominates the mixed water). Once an intrusion is detected, the depth of maximum salinity (ZS$_{max}$) indicates the shoreward intrusion branch. Based on ZS$_{max}$, we identify the top (Z$_t$) and bottom (Z$_b$) intrusion limits by using Equation 1 (adapted from Lentz (2003) for the SBB region):

$$S_{max} - S(z = z_{t,b}) = 0.75(S_{max} - S_{min}), \quad (1)$$

where S$_{max}$ is the maximum salinity detected in the vertical profile and S$_{min}$ is the minimum salinity found in the top/bottom intrusion layer, defining the upper and lower limits of the intrusion (in terms of depth, Z, and density, ρ). The difference between these two vertical positions will provide the intrusion thickness (δ) and the difference between S$_{max}$ and the bottom layer S$_{min}$ represents the salinity anomaly (ΔS), as illustrated by the average profiles in Fig. 2.

4.2. Statistical analysis

We test our entire dataset, i.e., vertical profiles with intrusions detected, for normality and homoscedasticity, using the Shapiro and Wilk (1965) and Levene (1961) tests, respectively. Since the dataset did not present a normal distribution, we applied non-parametric statistical analysis to describe the intrusions, considering a 95% confidence level of significance. To characterize the along-shelf and seasonal properties of the intrusions, we separate the intrusive dataset into compartments, as explained in Section 3 (Fig. 1), and seasons. The dataset does not have acceptably casts to ensure significance for the statistical tests for all four compartments (winter with 170, summer with 130, autumn with 93, and spring with 53 casts). Therefore, the temporal distribution was separated into summer/spring and winter/autumn, resulting in sufficient samples for each compartment. The occurrence was computed relative to the total vertical profiles available for each region and season. We used the Clopper–Pearson method to estimate the confidence intervals for frequency of occurrence, as it provides more accurate values for small samples (Suchéras-Marx et al., 2019). The characterization of the intrusions' properties was given by taking their median values and their confidence intervals. The along-shelf and seasonal differences were evaluated using the Mann–Whitney test at 95% of confidence level (hereafter, MW @ 95%CL). The confidence interval was established using the (Campbell and Gardner, 1988) method, considering the same confidence level. Some intrusions properties are negatively correlated to the stratification (e.g. Lentz, 2003). Therefore, we computed the Pearson correlation coefficient between the maximum salinity depth (ZS$_{max}$) and the maximum stratification depth (ZN$_{max}$), as well as the correlation between the thickness (δ) and the stratification itself (N^2). Both correlations use the 95% confidence level to ensure significance, and the confidence interval for the coefficient was obtained by applying the Fisher transformation. This analysis was made using the Pingouin package (Vallat, 2018).

4.3. Descriptive analysis

To identify if intrusions occur at pycnocline subsurface levels, we computed the ratio between the depth of maximum salinity (ZS$_{max}$) and the maximum stratification (ZN$_{max}$). If this ratio is approximately equal to 1, then intrusions occur near the pycnocline or near the bottom, if the ratio is higher than 1 (Lentz, 2003). During intrusive events, salty and warm waters (in the SBB case, TW) overlays cooler and relatively fresher waters (SACW) (Voorhis et al., 1976). This thermohaline structure tends to be favorable to double diffusion processes (Toole and Georgi, 1981; Ruddick and Walsh, 1995), which drives the mixing

of the intrusive waters with the surrounding waters. It is possible to evaluate the stratification susceptibility to double diffusion by applying the Turner Angle (Tu) analysis (Ruddick, 1983; Radko, 2013):

$$Tu = tg^{-1}\left(\frac{\alpha\Delta T - \beta\Delta S}{\alpha\Delta T + \beta\Delta S}\right), \quad (2)$$

where T is the temperature, S is the salinity, α is the coefficient of thermal expansion and β is the haline contraction coefficient. For Tu ranging from −90° to −45°, diffusive convection (DC) is possible, while angles varying between 45° and 90° indicate the possibility of salt fingering (SF). Between -45° and 45°, the water column is doubly stable (DS), stratified with respect to both temperature and salinity (You, 2002; Radko, 2013). This analysis provides a preliminary assessment of the chances of the occurrence of double diffusion during intrusive events. It is important to note that the analysis provides the necessary but insufficient conditions for double diffusion processes to occur (Radko, 2013).

Vertical shear tends to homogenize the water column, reducing the temperature and salinity variations vertically, therefore suppressing intrusions (Radko, 2013). To quantify the turbulence role over mixing within the intrusions, we applied the Bulk Richardson number adapted from Thomas et al. (2008) and given by:

$$Ri_b = \frac{< N^2 >_\rho \delta^2}{U^2} \quad (3)$$

where $< \cdot >_\rho$ is the isopycnal average stratification, considering the isopycnal boundaries of the intrusions, and δ is the intrusion thickness, both variables extracted from Table 2. The horizontal velocity is applied as a typical value (U) of 10^{-1} m s^{-1} (Dottori and Castro, 2009). Considering the different along shelf characteristics of SBB, we calculated Ri_b for the inner, mid and outer shelves (Castro, 2014), as well as for the MS and MN regions, considering both summer and winter.

5. Subsurface intrusions characterization

Vertical sections from two cruises from the Santos Project were used to evaluate the algorithm performance qualitatively. Transects with intrusions, detected visually, were compared with vertical profiles identified by the algorithm. A total of 23 vertical profiles were visually identified with intrusions, while the algorithm identified 20 casts, representing 87% of success rate.

5.1. Subsurface intrusions mean characteristics

In this section, we investigate the intrusions by evaluating their distribution of occurrence and features, such as absolute salinity, thickness and vertical core position. First, we present a general characterization, which introduces typical vertical profiles with intrusion, and then a seasonal characterization is presented.

Although the observations are not well distributed along the SBB and throughout the year, TW intrusions were identified over the entire shelf (27% of the vertical profiles analyzed, Fig. 3 a). The spatial variability presented a better confidence interval range (12.3%–18.34% and 33.7%–43.15%) in the central areas (Mid-northern and Mid-southern), due to a much higher density of observations. The Mid-Southern portion presented a significantly higher occurrence of intrusions than the Mid-Northern (38% and 15%, respectively), possibly related to relatively cold and fresher waters from continental runoff (e.g. Palma and Matano, 2009; Marta-Almeida et al., 2021). In addition, we observed significant (MW @ 95%CL) along-shelf variations in terms of S_{max} and its ZS_{max}, ΔS and vertical limits (Z_b, Z_t), which will be described in further detail.

To the north of SSI, the SBB presents a relatively narrow shelf, which allows more TW and SACW to influence the shelf, while the absence of large river discharges results in a smaller extent of CW (de Castro, 1996; Castro, 2014; Cerda and Castro, 2014). In this area, when downwelling-favorable winds are in place, surface onshore transport of TW is observed (Campos et al., 2000; Castro, 2014), which is displaced downwards by the CW presence nearshore due to density constraints. Consequently, in the northernmost areas, intrusions are shallower (21 m and 23 m) and saltier (36.9 g kg^{-1} and 36.42 g kg^{-1}), with higher salinity anomalies reaching 0.33 g kg^{-1} and 0.46 g kg^{-1}, respectively, for N and MN portions, but representing only 15% of occurrence. South of SSI, the southernmost areas are marked by a low salinity strip nearshore and a wider continental shelf, which prevents the Brazil Current from transporting oceanic waters to the mid-shelf (de Castro, 1996; Castro, 2014). The cross-shelf density gradient produced by the low salinities strip appears to be a necessary but not sufficient condition for the TW intrusions into the shelf, which might be related to the higher frequency of occurrence (38%). Moreover, these nearshore colder and fresher waters mix with warmer and saltier waters, producing fresher – 36.21 g kg^{-1} (36.19 g kg^{-1}) – and deeper – 37 m (24.5 m) – intrusions, with lower salinity anomalies that reach 0.19 g kg^{-1} (0.12 g kg^{-1}) for S (MS) regions.

The continental runoff south of the SBB is relevant for the low-salinity strip nearshore (basically CW), mainly in the S and MS areas (de Castro, 1996; Marta-Almeida et al., 2021). These contrasting situations may cause an overall deepening of the top limits of the intrusions, as observed in Fig. 4 (blue marker). From north to south, the top limit reaches depths of 21 to 10 m, approximately, and the southernmost intrusions are significantly (MW @ 95%CL) deeper (~10 m of difference) than the northernmost (Fig. 4), reinforcing this influence. The bottom limit also presents this same pattern, ranging from 35 m at N to 55 m at S. However, we found that shallower bottom limits at MS (35 m) differ significantly (MW @ 95%CL) from their neighboring regions (Fig. 4, red marker). In this region, we observed a squeezing pattern of the intrusive layer, probably as a response to upwelling favorable winds which bring SACW towards the coast (de Castro, 1996) elevating the bottom limit of the intrusion (Castro, 2014). Similarly, the increase in CW volume nearshore forces the top limit downwards, squeezing the intrusive layer, as exemplified by Fig. 5c.

Lentz (2003) found that intrusions are thinner when stratification is stronger, resulting in a negative correlation between thickness and stratification (N^2). In SBB, the same relationship was found, as evidenced by the Pearson correlation [-0.39, −0.18] (@ 95%CL). Looking further into the bottom and upper limits of the intrusion, we identified that this negative correlation occurs because the increase in CW volume above the intrusion causes a deepening of the superior limit. Below the intrusion, the presence of SACW forces the inferior limit upwards, possibly explaining the response found by the correlation. Consequently, thinner intrusions were found at N and MS (21 and 21.5 m, respectively), while thicker intrusions occurred at S and MN (36 and 34 m, respectively).

The thickness found within the SBB (Table 2) is consistent with the values collected by Ruddick and Richards (2003) for intrusions around the world. Note that the MS region presented a significant (MW @ 95%CL) thinner intrusion compared to the neighboring areas (S and MN), which could be a response to a local climatological presence of SACW near-bottom in this region.

5.2. Seasonal characterization

There was no significant seasonal variability of TW intrusion occurrences throughout the SBB at 95%CL (Fig. 3b), which could be a consequence of the number of available stations used in the analysis. Hence, by reducing the confidence level to 85%, the MN region presented significant seasonality, and winter showed a slightly higher frequency of intrusion occurrences than summer (18% and 13%, respectively). We acknowledge that CL at 85% for the occurrences is a relatively low standard in terms of significance, but the seasonal differences (significant at 95%CL) in the intrusion properties are encouraging evidence that this choice is appropriate, as presented in the

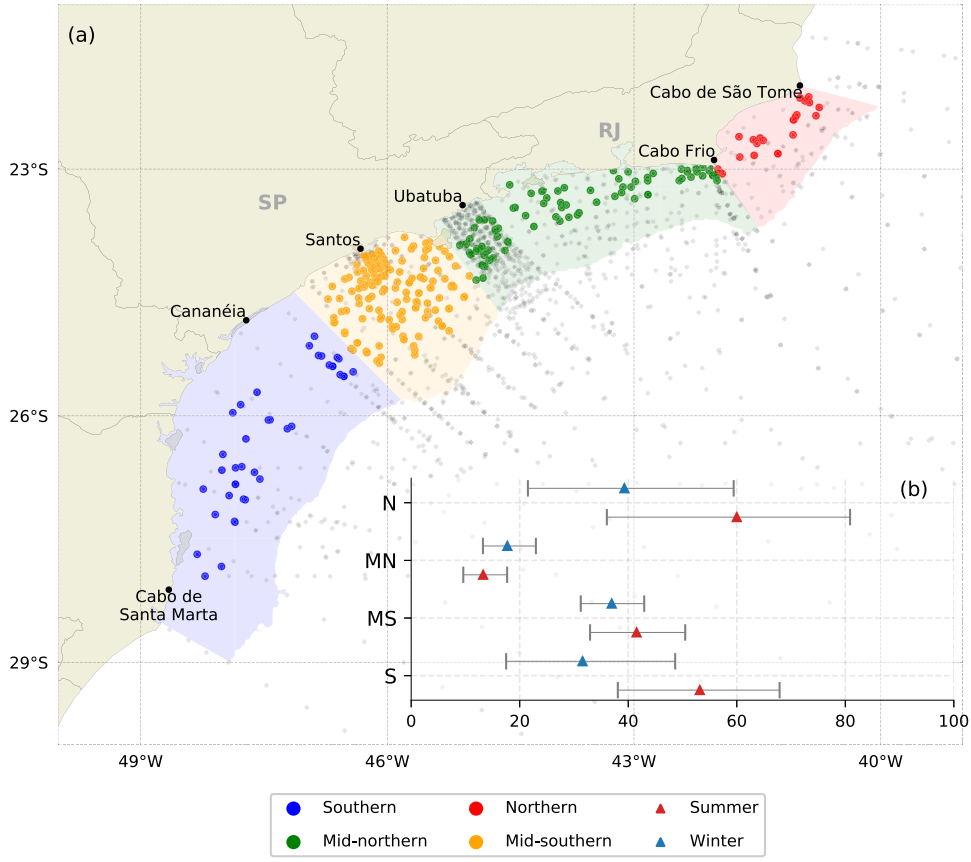

Fig. 3. Intrusive vertical profiles geographically distributed (a), separated by colors for each compartment. The inner bar graph (b) shows the proportional seasonal occurrence with confidence intervals for each region (in percentage). Red triangles represent the summer proportion, while blue triangles represent the winter. The background small dots in gray show all vertical profiles available from the historical dataset. Each compartment is bounded offshore by the 200 m isobath, even though only casts within the coastline and the 110 m isobath were considered in the detection.

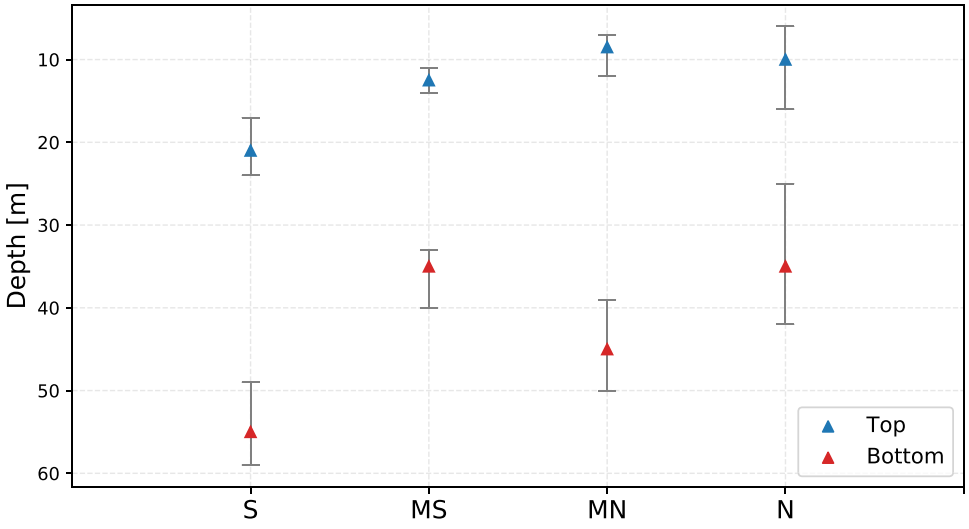

Fig. 4. Bar graph with the top (blue triangle) and bottom (red triangle) depth, separated by each compartment, along with the confidence interval.

coming paragraphs. The seasonal difference reflects the climatology presented by Castro (2014) for this area. During winter, there is a higher frequency of southwesterly winds that promotes a surface onshore transport of TW (Campos et al., 2000; Castro, 2014; Cerda and Castro, 2014), which might be related to the higher occurrence of intrusion in this season.

For MN, we found seasonal variability in the salinity anomalies, which were shallower in summer (15 m and 0.59 g kg^{-1}, respectively), relative to winter (33 m and 0.34 g kg^{-1}) in this same area. To the south of SSI, the MS region also presented intrusions that were shallower and thicker in summer (22 m and 24 m, respectively) relative to winter (28 m and 20 m, respectively). It is noteworthy the salinity anomaly in summer, which presented values of 0.3 g kg^{-1}, while winter showed smaller anomaly values (δS < 0.04 g kg^{-1}). This seasonality in salinity suggests a stronger intrusive signal during summer and, consequently, a larger TW volume during this season at MS. The same pattern was

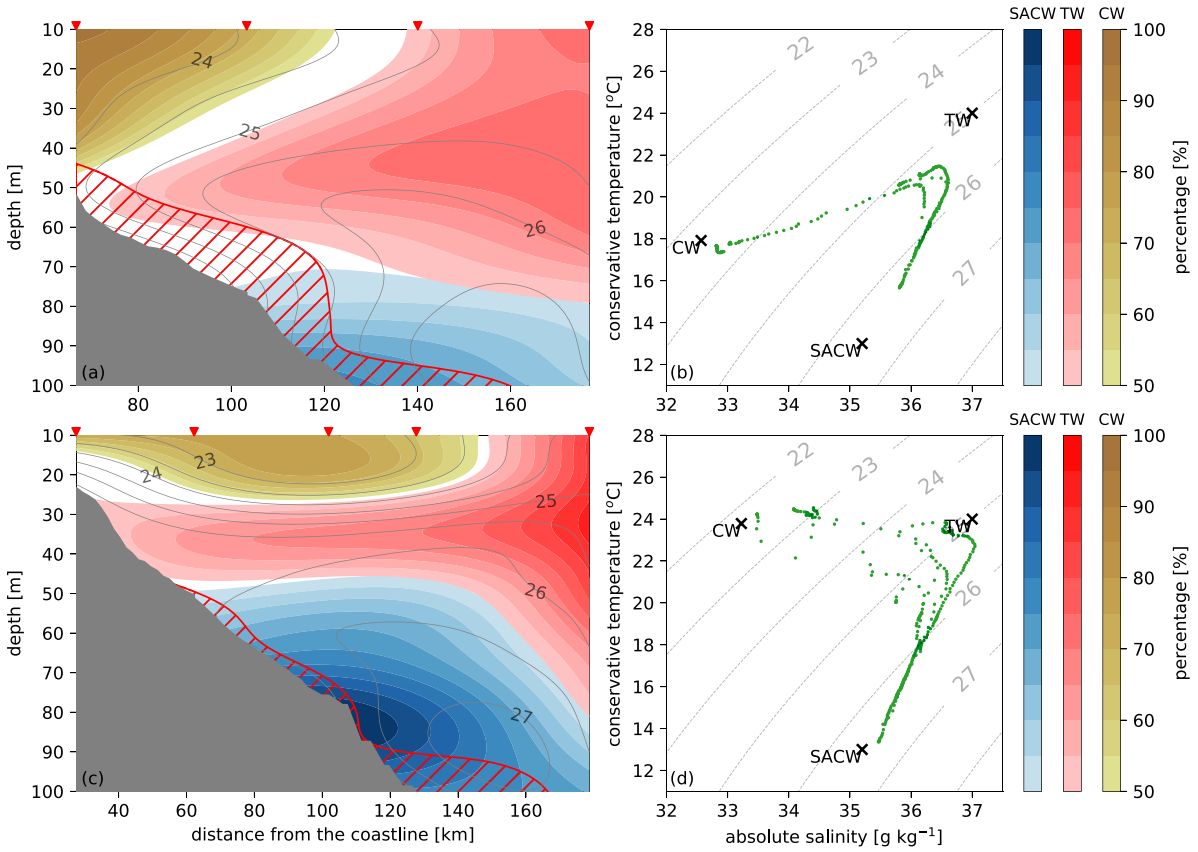

Fig. 5. Subsurface salty and warm intrusion transects (a, c) and respective T-S diagrams (b, d) in the South Brazil Bight (SBB). In (a) and (c), the colors represent the water masses: red is the Tropical Water (TW), blue is the South Atlantic Central Water (SACW) and yellow is the Coastal Water (CW). Each color gradient represents the amount, in percentage, of water with each water mass characteristic, following the method of the triangle of mixing from Mamayev (1975). White regions are placed where there was no dominance of a specific water mass (< 50%). The T-S diagrams, in (b) and (d), were constructed using the Absolute Salinity (in g kg^{-1}) and Conservative Temperature (in °C). The location of each water mass inserted into the diagrams corresponds to the hydrographic reference values for SACW and TW (Cerda and Castro, 2014). The CW hydrographic reference is based on the lowest absolute salinity found in the transect and its respective temperature. The gray lines in all panels are the isopycnals. Note that (c) is an example of the squeezing mechanism cited in the text.

found for the S region. All properties are presented in Table 2, even though some of them did not present significant seasonal differences. In terms of intrusions' properties, the Northern region did not present a significant seasonal variability, but the patterns found are similar to those in MN. Although N and MN are closer to each other, we cannot extend the seasonality found at MN to N, since these two regions have different characteristics, like the coastline orientation and shelf width (Castro and Miranda, 1998).

South of SSI (S+MS), winter presented the highest CW volume nearshore, due to the southwesterly wind regime, which brings low salinity waters from the south up to the SSI (Marta-Almeida et al., 2021). In this case, CW occupies the entire water column nearshore (Campos et al., 2000; Marta-Almeida et al., 2021), blocking the TW motion under CW in spite of the shoreward Ekman transport, which is a usual winter response to downwelling favorable winds at the SBB (Stech and Lorenzzetti, 1992; Campos et al., 2000). Thus, intrusions are more often found at the mid-shelf during winter, between 40 and 80 m (Fig. 6 a). They presented deeper intrusive cores (52.5 and 28 m) and reduced salinity anomalies (0.34 and 0.05 g kg^{-1}). During summer, SACW advance near the bottom in response to upwelling favorable winds (Campos et al., 2000; Palma and Matano, 2009) and CW volume reduces at the inner shelf (Marta-Almeida et al., 2021). This water mass arrangement possibly favors the TW intrusion in subsurface levels by creating a pathway between the CW and SACW (e.g. Fig. 5 a, c). As a result, intrusions found at the inner shelf (Fig. 6 a) are shallower (22 and 15 m) and show a higher salinity anomaly (0.28 and 0.59 g kg^{-1}) for S and MS respectively, suggesting a higher influence in the salt budget seasonality.

North of SSI (N+MN), we observed an opposite seasonal pattern. Intrusions hardly reach the inner shelf in both seasons, being restricted to the mid-shelf despite the stratification (Fig. 6b). During winter, CW reaches its lowest volume (Cerda and Castro, 2014), while the shelf becomes more homogeneous (Castro, 2014) and presents deeper intrusions, 26 m and 33 m, with smaller salinity anomalies, 0.32 g kg^{-1} and 0.34 g kg^{-1}, for N and MN respectively. During summer, there is an increase in the CW volume and a SACW shoreward near-bottom intrusion, which develops a stratified water column (Castro, 2014; Cerda and Castro, 2014). This arrangement of water masses creates a pathway for TW intrusions, which in this case are shallower (20 m at N and 15 m at MN) and show relatively higher salinity anomaly values (0.46 g kg^{-1} at N and 0.54 g kg^{-1} at MN) than winter. Cabo Frio region is known for the coastal upwelling during summer and spring with a SACW near-bottom intrusion, which is caused by a narrow continental shelf width (70 km), mesoscale activity on the slope, and NE upwelling favorable winds (Cerda and Castro, 2014; Palma and Matano, 2009). This spring–summer SACW uplifting and upwelling activity could be relevant in pushing the overlying TW intrusions to shallower depths when compared to the area south of SSI. Note that in spite of the configuration of water masses, intrusions are less frequent in summer than in winter.

The top limit (Table 2) of the intrusions is shallower in summer, 7 m and 9 m, than in winter, 12 m and 15 m, in MN and MS, respectively. The shallowest (deepest) limits coincide with the period of the reduced (increased) volume of CW, which might favor the upward (downward) advection of the top layer of the intrusion. The seasonality in the bottom limit of the intrusion was only significant (MW @ 95%CL)

Table 2
Median values for all features extracted from the intrusions detected by the algorithm and its confidence intervals in brackets for Summer and Winter. Gray cells represent seasons that differ significantly, at 95% confidence level.

Feature		N	MN	MS	S
S_{max} [g kg^{-1}]	**Summer**	37.01 [36.83 - 37.36]	36.52 [36.40 – 36.70]	36.21 [36.19 – 36.28]	36.24 [36.16 – 36.41]
	Winter	36.79 [36.44 - 38.91]	36.38 [36.31 – 36.56]	36.17 [36.13 – 36.20]	36.20 [36.14 – 36.60]
ZS_{max} [m]	**Summer**	20.00 [14.00 - 27.00]	**15.00 [13.00 – 21.00]**	**22.00 [21.00 – 24.00]**	**33.00 [31.00 – 39.00]**
	Winter	26.00 [18.00 – 63.00]	**33.00 [29.00 – 47.00]**	**28.00 [25.00 – 31.00]**	**52.50 [46.00 – 67.00]**
ΔS [g kg^{-1}]	**Summer**	0.46 [0.16 – 0.77]	**0.59 [0.51 – 0.71]**	**0.28 [0.23 – 0.38]**	**0.28 [0.19 – 0.61]**
	Winter	0.32 [0.25 – 0.88]	**0.34 [0.26 – 0.53]**	**0.05 [0.04 – 0.08]**	**0.01 [0.00 – 0.58]**
δ [m]	**Summer**	20.00 [11.00 – 29.00]	30.00 [24.00 – 39.00]	**24.00 [19.00 – 31.00]**	27.00 [24.00 – 47.00]
	Winter	29.00 [16.00 – 62.00]	35.00 [26.00 – 48.00]	**20.00 [17.00 – 24.00]**	40.00 [34.00 – 55.00]
ρ_t [kg m^{-3}]	**Summer**	24.68 [24.56 – 25.15]	24.29 [24.02 – 24.61]	**23.66 [23.33 – 24.12]**	**23.71 [23.45 – 23.84]**
	Winter	24.94 [23.91 – 25.63]	24.01 [23.61 – 24.56]	**23.99 [23.85 – 24.36]**	**24.65 [24.35 – 25.21]**
ρ_b [kg m^{-3}]	**Summer**	26.16 [26.03 - 26.58]	**26.51 [26.45 – 26.67]**	**26.32 [26.23 – 26.41]**	26.47 [26.23 – 26.55]
	Winter	26.31 [26.12 – 28.13]	**26.46 [26.34 – 26.53]**	**26.09 [25.97 – 26.18]**	25.99 [25.78 – 26.35]
z_t [m]	**Summer**	10.00 [6.00 – 16.00]	**7.00 [5.00 – 11.00]**	**9.00 [8.00 – 12.00]**	22.00 [17.00 – 24.00]
	Winter	9.00 [4.00 – 27.00]	**12.00 [8.00 – 18.00]**	**15.00 [13.00 – 16.00]**	20.00 [8.00 – 28.00]
z_b [m]	**Summer**	28.00 [21.00 – 43.00]	**39.00 [33.00 – 46.00]**	37.00 [31.00 – 44.00]	**53.00 [44.00 – 59.00]**
	Winter	36.00 [25.00 – 69.00]	**52.00 [46.00 – 60.00]**	35.00 [32.00 – 40.00]	**58.00 [54.00 – 67.00]**

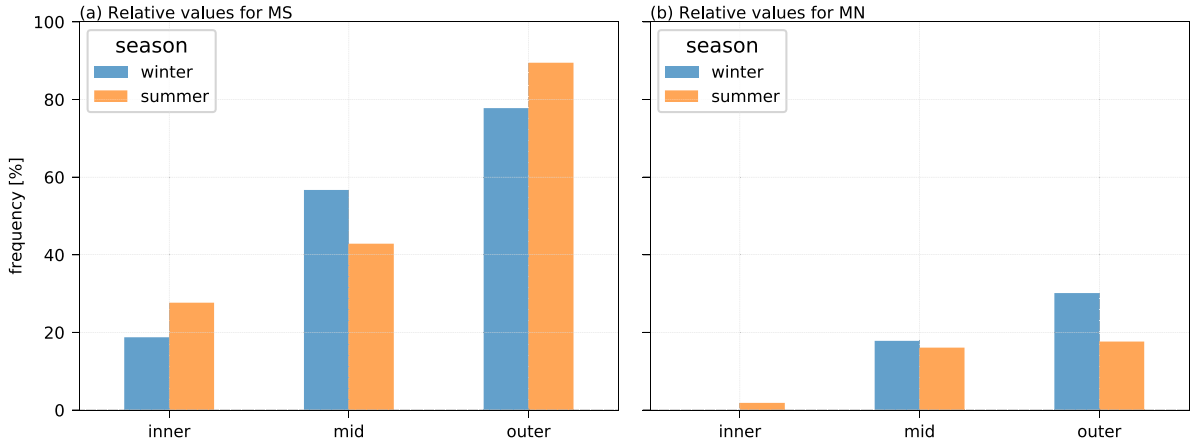

Fig. 6. Distribution of intrusions perpendicular to the coastline, classified in three compartments (inner, mid and outer shelf), according to Castro (2014) division, for Mid-Southern in (a) and Mid-Northern in (b). Colors represent summer (orange) and winter (blue). The percentage is calculated based on the total amount of intrusions in each compartment.

for the MN, with a shallower limit in summer (39 m) than in winter (52 m). Castro (2014) suggests that the SACW presence near-bottom in summer is responsible to uplift the intrusive TW layer in this same area, which reflects in shallower bottom limits in this season. As a consequence, the MN (MS) area presented thinner (thicker) intrusion in summer, differing mainly due to the topographic effect in MN, which favors an intense SACW advance (Cerda and Castro, 2014). Similar results were found by Palma and Matano (2009) in numerical simulations. In their study, the maximum salinity depth was shallower (deeper) and the thickness of the intrusion was thinner (thicker) in summer (winter), which was a consequence of SACW advance near the bottom in summer or due to an increase of CW volume nearshore in winter (see their Fig. 4). The differences found between southernmost and northernmost regions endorse the idea of an along-shelf difference in stratification (Miranda and Katsuragawa, 1991) and, therefore, the climatology developed by Castro (2014) and Cerda and Castro (2014) for the region north of SSI might present significant differences with respect to the region southward of SSI.

6. Double diffusive activity within the intrusions

The inverse relationship between stratification and thickness presented in Section 5.1 suggests that double diffusion processes may be associated with the intrusions, similarly to Lentz (2003). Since intrusions develop thermohaline structures favorable to these mixing processes, we dedicate this section to investigate the SBB environment susceptibility to double diffusion processes, based on the Turner Angle (Tu) probability density function (hereafter Tu pdf).

The Tu pdf suggests that the double-diffusion activity in SBB is independent of the presence of intrusions. (Fig. 7). However, different

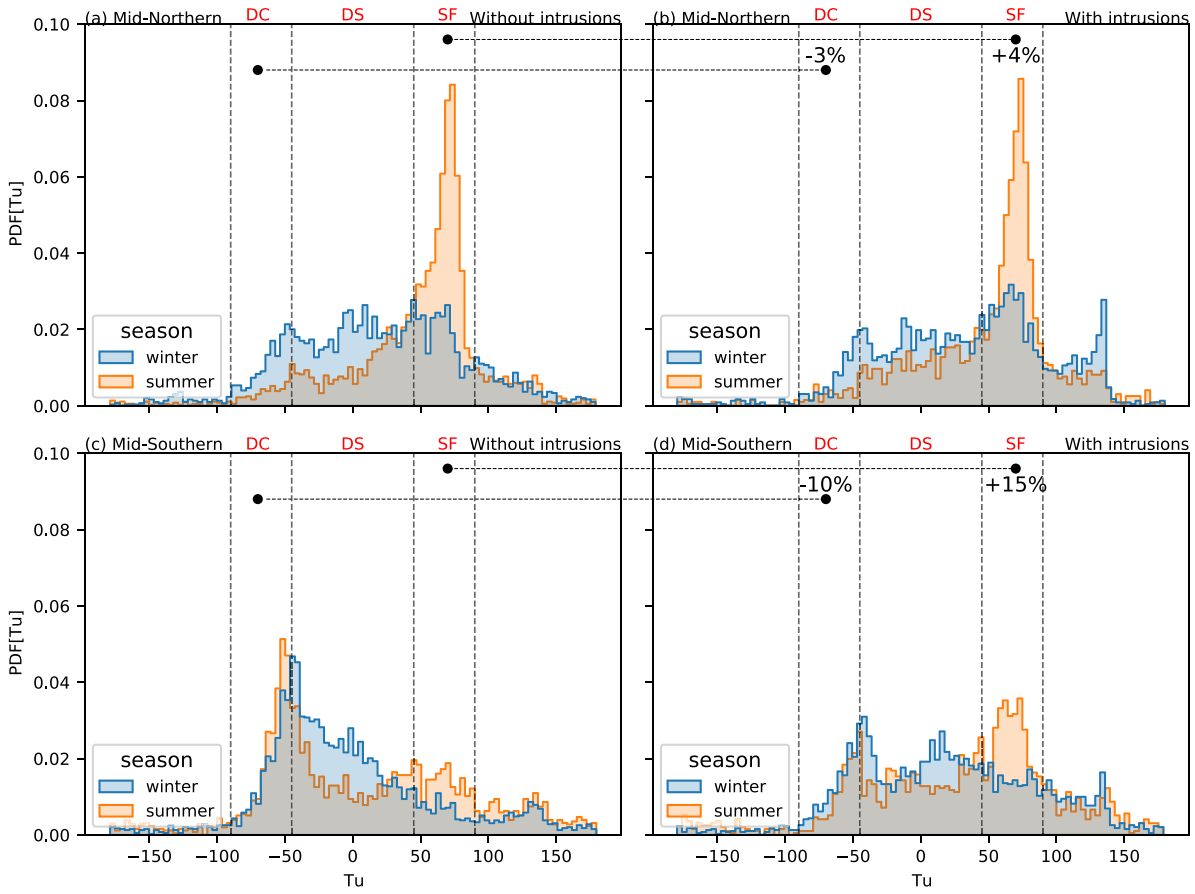

Fig. 7. Turner angle analysis probability density function (pdf). The upper panels show the Mid-Northern pdf without (a) and with (b) intrusions, while the lower panels present the distribution for the Mid-Southern region without (c) and with (d) intrusions. The orange color represents the summer distribution, while the blue is for winter.

along-shelf Tu pdf shapes were found, which are probably related to the environmental conditions south and north of SSI, as discussed in Section 5.2. Even though the Mid-Northern winter structure supports both forms of double diffusion (Fig. 7 a, b), about 42% and 48% of the distribution were found in the doubly stable (DS) range, with and without intrusions respectively. DS conditions occur when warm and fresher waters overlay colder and salty ones (Radko, 2013). In the SBB, this condition is found when CW overlays SACW. Therefore, the MN winter structure provides stable conditions without intrusions (approximately 48% of the Tu values were within the DS range). Beyond the 50-m isobath, the region also provides a thermohaline structure prone to SF, where the TW presence on top of SACW (Castro, 2014; Cerda and Castro, 2014) accounts for 23% of the occurrences. In addition, the warm and salty waters (TW) overlaying cold and relatively fresher waters (SACW), develops a thermohaline structure prone to salt fingering. This response is reflected in the Turner angle analysis as a peak in the salt fingering range (Fig. 7b), increasing to 29%. During summer, the thermohaline structure was favorable to salt fingering with (52%) or without (55%) intrusions (Fig. 7 a, b). Despite the increase in the CW volume nearshore in summer (Cerda and Castro, 2014), which favors diffusive convection, the interaction between TW and SACW appears to be dominant, promoting conditions for salt fingering.

The MS region contrasted with the MN region by presenting suitable environmental conditions for diffusive convection throughout the year with or without intrusions (Fig. 7c, d). The diffusive convection condition is a result of the quasi-permanent low-salinity strip nearshore (de Castro, 1996; Marta-Almeida et al., 2021), which creates an interface between CW and TW during winter, and between CW and TW (or SACW) during summer, as exemplified in Fig. 5 and also by the schematics proposed by Campos et al. (2000). Considering winter, the Tu pdf distribution at MS was approximately unimodal without intrusions (Fig. 7c) and became bimodal with intrusions (Fig. 7d). While in the first case, the first mode occurred at the limit between DC and DS conditions, the second mode of the second case was found around 0 and 35°, showing doubly stability. This difference between distributions suggests that the presence of intrusions tended to stabilize the environment. During summer, the bimodal pattern was preserved with and without intrusion (Fig. 7c, d), although with clear changes: Differently from winter, summer conditions supported not only diffusive convection (in smaller frequency, 12%) and doubly stability (36%), but also salt fingering (32%).

6.1. Double diffusion in the upper and bottom layers

Since the water mass composition in the SBB can generate unstable conditions for double diffusion (DC and SF) occurrence, it is possible for intrusions to present both double diffusion processes at their upper and lower boundaries (Ruddick and Walsh, 1995) due to the thermohaline vertical structure. In this case, the thermohaline structure favors the presence of diffusive convection in the upper layer, above the warm salty core (ZS_{max}), since relatively colder and fresher waters overlay warm and salty waters (Radko, 2013). Below ZS_{max}, the bottom layer can be unstable to salt fingering, due to warm and salty waters overlaying cooler and relatively fresher waters (Voorhis et al., 1976; Posmentier and Houghton, 1978). The different processes suggest that double diffusion, in fact, might play an important role in the intrusion growth and steady-state stages and in the vertical mixing (May and Kelley, 2002; Ruddick and Richards, 2003; Beal, 2007). Therefore, it is useful to evaluate the double diffusion activity in both the upper

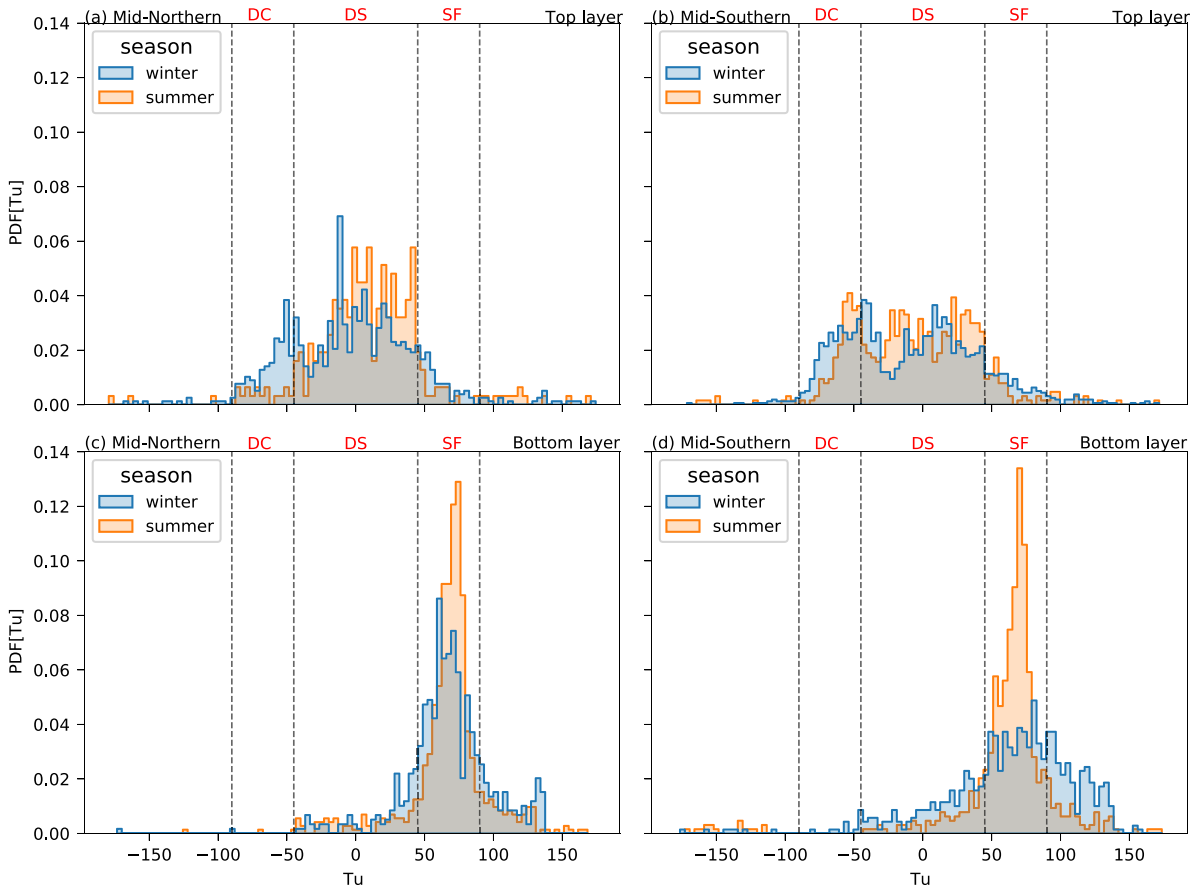

Fig. 8. Turner angle analysis probability density function (pdf). The upper panels show the top layer distribution for Mid-Northern (a) and Mid-Southern (b), while the lower panels show the bottom layer distribution for Mid-Northern (c) and Mid-Southern (d). The orange color represents the summer distribution, while the blue is for winter.

and bottom layers of the intrusion, separated by the maximum salinity depth (ZS_{max}).

The Tu pdf for the MN region showed a region with a doubly stable environment throughout the year, even though the skewness of the distribution denoted an environment with conditions susceptible to double diffusion processes. In summer (Fig. 8a), the interface between CW and SACW is higher due to the increase in CW volume and the coastal upwelling (Castro, 2014; Cerda and Castro, 2014). This interface generates a strong stratification (Castro, 2014) which tends to stabilize the water column. Nevertheless, the TW and SACW interface still exist independently of intrusions, although at larger distances from the coast (from the mid-shelf or 50-m isobath), which generates environmental conditions to support salt fingering. This interaction might be the reason the Tu pdf was slightly skewed to the salt fingering side in summer. In winter, the Tu pdf was bimodal (Fig. 8a). The first peak was found in the diffusive convection side (13% of occurrence against 1% in summer), which is possibly related to the buoyancy advection of low salinity waters from south of SSI (Castro, 2014) and concentrates near the boundary between MN and MS (not shown). The second peak occurred in the doubly stable range.

The environmental condition in MS presented a clearer bimodal pattern (Fig. 8b) throughout the year. The first peak, skewed to diffusive convection, is a response to the semi-permanent CW presence nearshore observed in the region (de Castro, 1996; Marta-Almeida et al., 2021). In winter, when CW volume is higher, there was a slightly higher peak (from 6% to 18% of occurrences) in the diffusive convection, relative to summer. The second peak, concentrated approximately at 0°, shows a region doubly stable in both summer and winter. At the bottom half of the intrusion, where TW - salty and warm - overlay SACW - relatively fresher and cooler -, salt fingering processes are possible to occur, as suggested by the Tu pdf for both winter and summer and both regions (Fig. 8b and d). However, winter presented a lower peak (30% and 22.5% for MN and MS, respectively) relative to summer (42.3% and 35.8%), and an increase in the doubly stable range (1% and 6%, for MN and MS). The highest CW volume, which occurred in winter at MS, tends to stabilize the water column since the CW occupies the entire water column (Fig. 5a), reducing the SF occurrences (Fig. 8d).

6.2. Are these intrusions double-diffusively driven?

The inverse relationship between stratification and thickness (Section 5) suggests that intrusions at the SBB might be double-diffusively driven (Ruddick and Turner, 1979; Lentz, 2003). Therefore, it is insightful to investigate if the characteristics of the intrusions, e.g., thickness and nose velocity (i.e., the velocity of the shoreward edge of the intrusion, found by the S_{max}), are similar to those predicted by theoretical studies. The thickness, or vertical scale (δ), for double-diffusively driven intrusions, was introduced by Ruddick and Turner (1979) as a function of hydrographic data by:

$$\delta = \frac{3}{2}(1-n)\frac{g\beta\Delta S}{N^2}, \tag{4}$$

where n is the density flux ratio across the intrusion (0.56 for salt fingering, Ruddick and Turner, 1979) and g is the gravitational acceleration, approximately 9.8 m s^{-2}. Applying the averaged values from verticals profiles with intrusions, like N^2 of 2.8 × 10^{-4} s^{-2}, haline contraction coefficient (β) of 7.6 × 10^{-4} g kg^{-1} and ΔS of 0.3 g kg^{-1}, the vertical length (δ) is about 5 m.

Table 3
Bulk Richardson number using the formulation of Thomas et al. (2008) adapted to consider the isopycnal averaged stratification inside the intrusion ($<N^2>$, in s^{-1}), the intrusion thickness (δ in m) and the characteristic horizontal velocity (U) of 10^{-1} m s^{-1} (Dottori and Castro, 2009). The values were calculated considering the inner, mid and outer shelves (Castro, 2014), where H is the local depth, for summer and winter of the MN and MS regions (Fig. 1).

		Inner (20 < H < 40 m)	Mid (40 < H < 80 m)	Outer (80 < H < 110 m)
Mid-Northern	Summer	2.08	3.55	5.63
	Winter	3.18	3.71	5.07
Mid-Southern	Summer	2.66	4.15	8.65
	Winter	2.14	3.89	7.12

This order of magnitude found by the predicted thickness is inconsistent with the average values found in Section 5 (of 15 to 40 m). Thus, this difference suggests that SBB intrusions are not initially double-diffusively driven, although these processes may act during the development of the intrusion. It is also possible to scale the normal nose velocity of a double diffusive driven intrusion by c = 0.0005 N δ, as introduced by Ruddick and Turner (1979). Taking the same N and the values of thickness (as δ) from Section 5, the predicted velocities vary from 0.4 to 1 mm s^{-1}. Observationally, we estimated the intrusive core velocity using the DEPROAS daily measurements of a hydrographic transect normal to the coast of the Cabo Frio region, where an intrusion growth was detected. By tracking the cross-shore distance traveled by the 36-isohaline, we estimated an intrusion moving with, approximately, 183 mm s^{-1}. The difference between observational and predicted velocities also suggests that the process triggering the salty and warm intrusions at the SBB was not double-diffusion driven. The SBB was always susceptible to double diffusion, independently of intrusions, according to the Tu pdf analysis for the entire water column (Section 6). In this case, we expected intrusions to occur at a much higher frequency than the one found (27%), supporting the hypothesis that double diffusion may take no part in triggering the intrusions. In spite of this, it is possible that double diffusion influence the intrusion growth and steady-state (May and Kelley, 1997, 2002; Beal, 2007), as discussed by other studies around the world (Ruddick and Bennett, 1985; Schmitt et al., 1986; May and Kelley, 2002; Beal, 2007).

The role of the double diffusion becomes evident when analyzing the Turner Angle in the upper and lower layers of the intrusion (Section 6.1). The upper half of the intrusion presents, in general, a thermohaline structure represented by cooler and fresher waters (CW) overlying warm and salty (TW). This condition turns the upper layer unstable to diffusive convection (Fig. 8a, b). In this case, the intrusion loses heat and gains salt, increasing its density. As a consequence, along the intrusion, the isopycnals slope downward (Ruddick and Walsh, 1995) toward the coast, sinking below CW (note the isopycnals in Fig. 5). The lower half of the intrusion presents the opposite condition, with warm and salty waters (TW) overlying cooler and relatively fresher waters (SACW). It results in a bottom half susceptible to salt fingering (Fig. 8c, d), which removes heat and salt from the intrusion, making it less dense. As a consequence, the isopycnals slope upward (Ruddick and Walsh, 1995) towards the coast. Therefore, the TW intrusion will rise above SACW as the intrusion moves towards the coast (note the isopycnals in Fig. 5). When double diffusion dominates the growth or steady-state stages, the intrusive layer will slope relative to geopotential surfaces, with the angle signal varying according to the dominant process (May and Kelley, 2002; Ruddick and Richards, 2003; Beal, 2007). Based on the results presented, the Tu distribution at each half of the intrusion provides evidence that double diffusion may play a role in the development of intrusions in the region.

Double diffusion and shear-driven mixing can coexist in the same region, although their interaction is still unclear (Ruddick and Richards, 2003). The turbulence can either suppress (Zhurbas and Oh, 2001) or enhance the intrusive growth (Kuzmina and Rodionov, 1992; May and Kelley, 1997; Kuzmina and Zhurbas, 2000; Walsh and Ruddick, 2000), which will influence the vertical fluxes (Garrett, 1982; Hebert, 1988). The turbulence role over mixing within intrusions was quantified through the Bulk Richardson number (Ri_b). The results (Table 3) shows Ri_b of O (10) and always higher than the critical Ri of 1/4 (Miles, 1961). It indicates that mixing is not shear-driven, because the stratification suppresses the vertical shear turbulence (Bebieva and Timmermans, 2016). Therefore, double diffusion processes have the potential of mixing the intrusive layer with surrounding waters on the continental shelf.

7. Conclusion

In this study, we investigated the occurrence and the main features of a tongue-shaped structure of salty and warm waters found at the South Brazil Bight (Campos et al., 2000; Palma and Matano, 2009; Castro, 2014). By applying a detection algorithm (Lentz, 2003), we identified that these structures occur in 27% of a historical hydrographic dataset between the coast and the 110-m isobath (inner and mid-shelves). Intrusions are more likely to be found south of São Sebastião Island (SSI) compared to the north of it, differing significantly (@ 95%CL) in occurrence between MN and MS. These differences are related to the Coastal Water (CW) and South Atlantic Central Water (SACW) presence along the shelf, affecting the characteristics of the intrusions. Higher CW volume south of SSI relative to north forces intrusions to present deeper patterns. The mixing between TW and CW produces relatively fresher intrusions when compared to the north, where the reduced CW volume produces shallower and saltier intrusions. On the other hand, near-bottom SACW presence forces intrusions to be shallower north of SSI, where SACW advances towards the coast more effectively (Castro, 2014; Cerda and Castro, 2014). When both water masses are found simultaneously, which means a more stratified water column, intrusions are thinner. This reflects a negative correlation between intrusions' thickness and stratification.

This inverse relation suggests double-diffusively driven intrusions (Ruddick and Turner, 1979; Lentz, 2003). When analyzing the Turner Angle (Tu, Lentz, 2003), we found that the SBB is always susceptible to such processes, with or without intrusions. In addition, we compared theoretical thickness and nose velocity with our dataset. The differences between them suggest that intrusions are not initially double-diffusively driven. Nevertheless, we also found that different double diffusion processes occurred at the upper and lower boundaries of the intrusion. These differences may affect intrusion dynamics, leading to growth, stability, or even erosion (Beal, 2007; Shcherbina et al., 2010).

Our findings are summarized in Fig. 9, which shows along-shelf and seasonal differences in the intrusions' features and double diffusion processes occurring at the upper and lower layers of the intrusion, considering the MS and MN regions. These results leave us with open questions about which mechanism is responsible for triggering the initial density perturbation that will evolve into an intrusion. Our results are comparable to other regions where similar relations - double diffusion not triggering intrusions but affecting their dynamics - have been described, like in the Agulhas Current system (Beal, 2007), the Gulf Stream (Ruddick and Bennett, 1985; Schmitt et al., 1986) and the Arctic Ocean (May and Kelley, 2002). Therefore, further work is needed to identify the mechanisms involved in generating these intrusions, as well as investigate how these structures mix with surrounding waters.

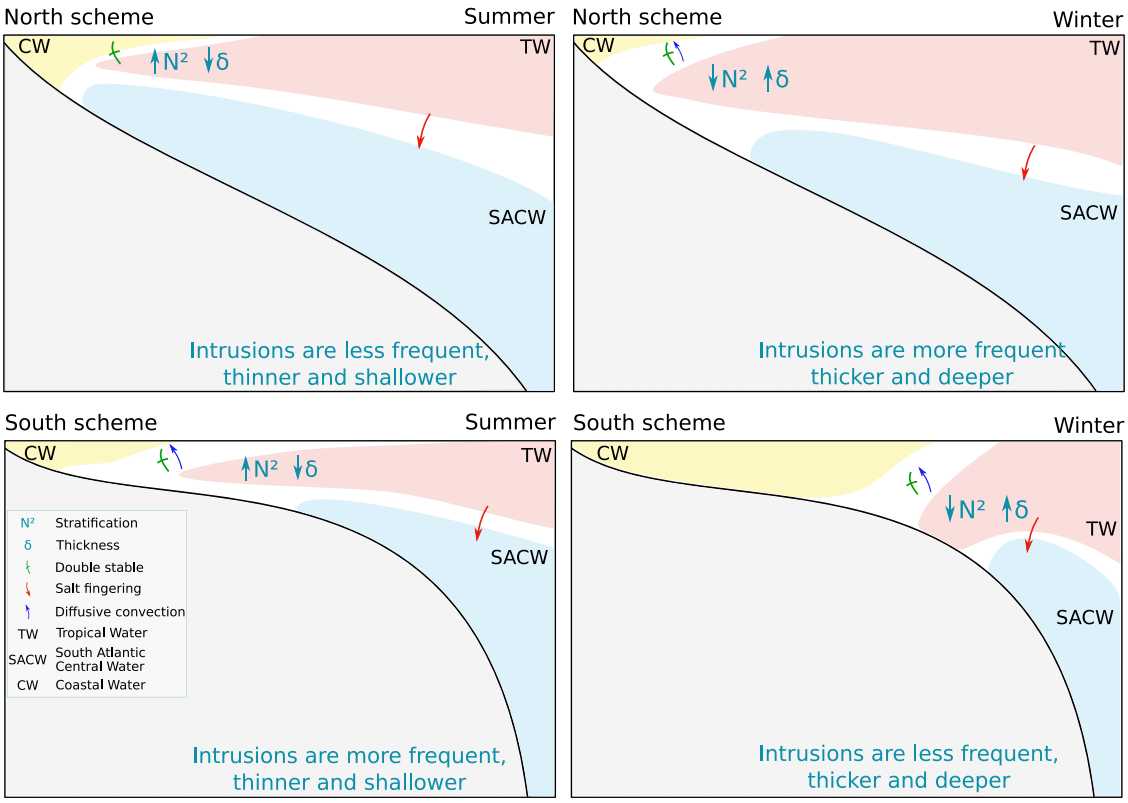

Fig. 9. Schemes that summarize the findings of this study for the northern (upper panels) and southern (lower panels) parts of the South Brazil Bight, divided by the São Sebastião Island. The left (right) columns represents the Summer (Winter) conditions. Colored shapes stands for the three water masses found in the SBB: blue is the South Atlantic Central Water (SACW), red is the Tropical Water (TW) and yellow is the Coastal Water (CW).

CRediT authorship contribution statement

Danilo Augusto Silva: Conception and design of study, Analysis and interpretation of data, Writing – original draft, Writing – review & editing. **Dalton Kei Sasaki:** Conception and design of study, Analysis and/or interpretation of data, Writing – original draft, Writing – review & editing. **Marcelo Dottori:** Conception and design of study, Analysis and/or interpretation of data, Writing – original draft, Writing – review & editing. **Ilson Carlos Almeida da Silveira:** Analysis and/or interpretation of data, Writing – review & editing. **Wellington Ceccopieri Belo:** Writing – review & editing. **Renato Parkinson Martins:** Writing – review & editing.

Declaration of competing interest

The authors declare the following financial interests/personal relationships which may be considered as potential competing interests: Danilo A. Silva reports financial support was provided by Petrobras. Dalton K. Sasaki reports financial support was provided by Petrobras. Marcelo Dottori reports financial support was provided by Petrobras. Ilson C. A. da Silveira reports financial support was provided by Petrobras.

Acknowledgments

We thank Petróleo Brasileiro S.A. (PETROBRAS) for their permission to use and display the proprietary data from Santos Project – Santos Basin Environmental Characterization – for this paper. This study also makes use of an observational dataset kindly provided by the Brazilian Navy. The authors would like to thank all these organizations for making the dataset available. Danilo A. Silva and Dalton K. Sasaki acknowledge financial support from PETROBRAS (Santos Project, 2018/00068-8), Marcelo Dottori acknowledges support from the Fundação de Amparo à Pesquisa do Estado de São Paulo (FAPESP 2010/05124-1) and Ilson Carlos Almeida da Silveira acknowledges support from CNPq (Project HIDROSAN I, 405593/2021-0) and FAPESP (Project HIDROSAN II, 2021/13124-6). We also thank the reviewers for their valuable suggestions and comments, which considerably improved the quality of this article.

References

Beal, L.M., 2007. Is interleaving in the Agulhas Current driven by near-inertial velocity perturbations? J. Phys. Oceanogr. 37, 932–945. http://dx.doi.org/10.1175/JPO3040.1.

Bebieva, Y., Timmermans, M.L., 2016. An examination of double-diffusive processes in a mesoscale eddy in the Arctic Ocean. J. Geophys. Res.: Oceans 121, 457–475. http://dx.doi.org/10.1002/2015JC011105.

Bianchi, A.A., Giulivi, C.F., Piola, A.R., 1993. Mixing in the Brazil-Malvinas confluence. Deep-Sea Res. I 40, 1345–1358. http://dx.doi.org/10.1016/0967-0637(93)90115-J.

Boyd, T.J., D'Asaro, E.A., 1994. Cooling of the West Spitsbergen Current: Wintertime observations West of Svalbard. J. Geophys. Res.: Oceans 99, 22597–22618. http://dx.doi.org/10.1029/94JC01824.

Campbell, M.J., Gardner, M.J., 1988. Statistics in Medicine: Calculating confidence intervals for some non-parametric analyses. Br. Med. J. (Clinical Research Ed.) 296 (6634), 1454. http://dx.doi.org/10.1136/BMJ.296.6634.1454.

Campos, E.J., Velhote, D., Silveira, I.C.D., 2000. Shelf break upwelling driven by Brazil current cyclonic meanders. Geophys. Res. Lett. 27, 751–754. http://dx.doi.org/10.1029/1999GL010502.

Castelao, R., 2011. Intrusions of Gulf Stream waters onto the South Atlantic Bight shelf. J. Geophys. Res.: Oceans 116, 10011. http://dx.doi.org/10.1029/2011JC007178.

de Castro, B.M., 1996. Correntes e massas de água da plataforma continental norte de São Paulo. Livre-Docente Thesis. Instituto Oceanográfico Da Universidade de São Paulo.

Castro, B.M., 2014. Summer/winter stratification variability in the central part of the South Brazil Bight. Cont. Shelf Res. 89, 15–23. http://dx.doi.org/10.1016/j.csr.2013.12.002.

Castro, B.d., Miranda, L.d., 1998. Physical oceanography of the western Atlantic continental shelf located between 4N and 34S. The Sea 11 (1), 209–251.

Castro, B.M., Miranda, L.B., Silva, L.S., Fontes, R.F.C.., Pereira, A.F., Coelho, A.L., 2008. Processos físicos: Hidrografia, circulação e transporte. EDUSP, pp. 59–121,

Cerda, C., Castro, B.M., 2014. Hydrographic climatology of South Brazil Bight shelf waters between Sao Sebastiao (24°S) and Cabo Sao Tome (22°S). Cont. Shelf Res. 89, 5–14. http://dx.doi.org/10.1016/j.csr.2013.11.003.

Dottori, M., Castro, B.M., 2009. The response of the Sao Paulo continental shelf, Brazil, to synoptic winds. Ocean Dyn. 59 (4), 603–614. http://dx.doi.org/10.1007/s10236-009-0209-2.

Dottori, M., Castro, B.M., 2018. The role of remote wind forcing in the subinertial current variability in the central and northern parts of the South Brazil Bight. Ocean Dyn. 68 (6), 677–688. http://dx.doi.org/10.1007/s10236-018-1153-9.

Dottori, M., Sasaki, D.K., Silva, D.A., Del-Giovannino, S.R., Pinto, A.P., Gnamah, M., Santos, A.D., Silveira, I.C.A.d., Belo, W.C., Martins, R.P., et al., 2023. Hydrographic structure of the continental shelf in Santos Basin and its causes: The SANAGU and SANSED campaigns (2019). Ocean and Coastal Res. 71 (suppl 3), http://dx.doi.org/10.1590/2675-2824071.22062md.

Fernandes, F., 2014. Python-ctd v0.2.1. http://dx.doi.org/10.5281/zenodo.11396.

Fontes, R.F.C., de Castro, B.M., 2017. Currents on the continental shelf adjacent to the Laje de Santos (SP, Brazil). Braz. J. Oceanogr. 65, 595–604.

Garrett, C., 1982. On the parameterization of diapycnal fluxes due to double-diffusive intrusions. J. Phys. Oceanogr. 12, 952–959. http://dx.doi.org/10.1175/1520-0485(1982)012<0952:OTPODF>2.0.CO;2.

Georgi, D.T., 1981. On the relationship between the large-scale property variations and fine structure in the Circumpolar Deep Water. J. Geophys. Res.: Oceans 86, 6556–6566. http://dx.doi.org/10.1029/JC086IC07P06556.

González-Pola, C., Ruiz-Villarreal, M., Lavín, A., Cabanas, J.M., Álvarez-Fanjul, E., 2007. A subtropical water intrusion spring-event in the shelf-slope of the south-western Bay of Biscay after strong wind-forcing pulses. J. Atmos. Ocean Sci. 10, 343–359. http://dx.doi.org/10.1080/17417530601129148.

Hebert, D., 1988. Estimates of salt-finger fluxes. Deep-Sea Res. A 35, 1887–1901. http://dx.doi.org/10.1016/0198-0149(88)90115-X.

Hopkins, J., Sharples, J., Huthnance, J.M., 2012. On-shelf transport of slope water lenses within the seasonal pycnocline. Geophys. Res. Lett. 39, http://dx.doi.org/10.1029/2012GL051388.

Jan, S., Wang, S.H., Yang, K.C., Yang, Y.J., Chang, M.H., 2019. Glider observations of interleaving layers beneath the kuroshio primary velocity core east of taiwan and analyses of underlying dynamics. Sci. Rep. 9, 1–11. http://dx.doi.org/10.1038/s41598-019-47912-z.

Joyce, T.M., Zenk, W., Toole, J.M., 1978. The anatomy of the Antarctic polar front in the Drake Passage. J. Geophys. Res.: Oceans 83, 6093–6113. http://dx.doi.org/10.1029/JC083IC12P06093.

Katsuragawa, M., Dias, J.F., Harari, J., Namiki, C., Zani-Teixeira, M.L., 2014. Patterns in larval fish assemblages under the influence of the Brazil current. Cont. Shelf Res. 89, 103–117. http://dx.doi.org/10.1016/J.CSR.2014.04.024.

Kuzmina, N.P., Rodionov, V.B., 1992. Influence of baroclinicity on formation of thermohaline intrusions in ocean frontal zones. Am. Geophys. Union 28.

Kuzmina, N., Zhurbas, V., 2000. Effects of double diffusion and turbulence on interleaving at baroclinic oceanic fronts. J. Phys. Oceanogr. 30 (12), 3025–3038.

Lentz, S., 2003. A climatology of salty intrusions over the continental shelf from Georges Bank to Cape Hatteras. J. Geophys. Res.: Oceans 108, http://dx.doi.org/10.1029/2003jc001859.

Levene, H., 1961. Robust tests for equality of variances. Contributions To Probability and Statistics. Essays in Honor of Harold Hotelling 279–292.

Li, Y., Wang, F., Sun, Y., 2012. Low-frequency spiciness variations in the tropical Pacific Ocean observed during 2003–2012. Geophys. Res. Lett. 39, http://dx.doi.org/10.1029/2012GL053971.

Mahiques, M.M.D., Tessler, M.G., Ciotti, A.M., Silveira, I.C.A.D., Sousa, S.H.D.M.E., Figueira, R.C.L., Tassinari, C.C.G., Furtado, V.V., Passos, R.F., 2004. Hydrodynamically driven patterns of recent sedimentation in the shelf and upper slope off Southeast Brazil. Cont. Shelf Res. 24, 1685–1697. http://dx.doi.org/10.1016/J.CSR.2004.05.013.

Malan, N., Archer, M., Roughan, M., Cetina-Heredia, P., Hemming, M., Rocha, C., Schaeffer, A., Suthers, I., Queiroz, E., 2020. Eddy-driven cross-shelf transport in the east Australian current separation zone. J. Geophys. Res.: Oceans 125, http://dx.doi.org/10.1029/2019JC015613.

Mamayev, O.I., 1975. Temperature-Salinity Analysis of World Ocean Waters. Elsevier.

Marta-Almeida, M., Dalbosco, A., Franco, D., Ruiz-Villarreal, M., 2021. Dynamics of river plumes in the South Brazilian Bight and South Brazil. Ocean Dyn. 71, 59–80. http://dx.doi.org/10.1007/S10236-020-01397-X/FIGURES/12.

May, B.D., Kelley, D.E., 1997. Effect of baroclinicity on double-diffusive interleaving. J. Phys. Oceanogr. 27, 1997–2008.

May, B., Kelley, D.E., 2002. Contrasting the interleaving in two baroclinic ocean fronts. Dyn. Atmos. Oceans 36, 23–42. http://dx.doi.org/10.1016/S0377-0265(02)00023-4.

Miles, J.W., 1961. On the stability of heterogeneous shear flows. J. Fluid Mech. 10 (4), 496–508.

Miranda, L.B., 1982. Análise de massas de água da plataforma continental e da região oceânica adjacente: Cabo de são tomé (RJ) a ilha de são sebastião (SP). Livre DocÊncia Thesis. Universidade de Sao Paulo.

Miranda, L.d., Katsuragawa, M., 1991. Estrutura térmica na região sudeste do Brasil (outubro/novembro de 1988). Publ. Esp. Inst. Oceanogr. 8, 1–14.

Muhling, B.A., Beckley, L.E., Koslow, J.A., Pearce, A.F., 2008. Larval fish assemblages and water mass structure off the oligotrophic south-western Australian coast. Fisheries Oceanography 17, 16–31. http://dx.doi.org/10.1111/J.1365-2419.2007.00452.X.

Namiki, C., Katsuragawa, M., Napolitano, D.C., de Lourdes Zani-Teixeira, M., de Mattos, R.A., da Silveira, I.C.A., 2017. Hydrodynamically-driven distribution of lanternfish larvae in the Southeast Brazilian Bight. J. Mar. Syst. 170, 115–133. http://dx.doi.org/10.1016/J.JMARSYS.2017.02.006.

Olivar, P.M., Shelton, P.A., 1993. Larval fish assemblages of the Benguela Current. Bull. Mar. Sci. 53 (2), 450–474.

Palma, E.D., Matano, R.P., 2009. Disentangling the upwelling mechanisms of the South Brazil Bight. Cont. Shelf Res. 29 (11–12), 1525–1534.

Perkin, R.G., Lewis, E.L., 1984. Mixing in the West Spitsbergen Current. J. Phys. Oceanogr. 14, 1315–1325. http://dx.doi.org/10.1175/1520-0485(1984)014<1315:MITWSC>2.0.CO;2.

Piola, A.R., 2005. The influence of the Plata River discharge on the western South Atlantic shelf. Geophys. Res. Lett. 32, L01603. http://dx.doi.org/10.1029/2004GL021638.

Piola, A.R., Georgi, D.T., 1982. Circumpolar properties of Antarctic intermediate water and Subantarctic Mode Water. Deep-Sea Res. A 29, 687–711. http://dx.doi.org/10.1016/0198-0149(82)90002-4.

Posmentier, E.S., Houghton, R.W., 1978. Fine structure instabilities induced by double diffusion in the shelf/slope water front. J. Geophys. Res.: Oceans 83 (C10), 5135–5138. http://dx.doi.org/10.1029/JC083IC10P05135.

Provost, C., Gana, S., Garçon, V., Maamaatuaiahutapu, K., England, M., 1995. Hydrographic conditions in the Brazil-Malvinas confluence during austral summer 1990. J. Geophys. Res.: Oceans 100, 10655–10678. http://dx.doi.org/10.1029/94JC02864.

Radko, T., 2013. Double-Diffusive Convection. Cambridge University Press.

Robertson, R., Padman, L., Levine, M.D., 1995. Fine structure, microstructure, and vertical mixing processes in the upper ocean in the western Weddell Sea. J. Geophys. Res.: Oceans 100, 18517–18535. http://dx.doi.org/10.1029/95JC01742.

Roden, G.I., 1964. Oceanographic aspects of Gulf of California1. In: Marine Geology of the Gulf of California: A Symposium. 10.1306/M3359C2, American Association of Petroleum Geologists, pp. 30–58. http://dx.doi.org/10.1306/M3359C2.

Ruddick, B., 1983. A practical indicator of the stability of the water column to double-diffusive activity. Deep-Sea Res. A 30 (10), 1105–1107.

Ruddick, B.R., Bennett, A.S., 1985. Fine structure and mixing at the edge of a warm core ring. J. Geophys. Res.: Oceans 90, 8943–8951. http://dx.doi.org/10.1029/JC090IC05P08943.

Ruddick, B., Hebert, D., 1988. The mixing of meddy “Sharon”. Elsevier Oceanography Series 46, 249–261. http://dx.doi.org/10.1016/S0422-9894(08)70551-8.

Ruddick, B., Richards, K., 2003. Oceanic thermohaline intrusions: observations. Prog. Oceanogr. 56 (3), 499–527. http://dx.doi.org/10.1016/S0079-6611(03)00028-4, Double-Diffusion in Oceanography.

Ruddick, B.R., Turner, J.S., 1979. The vertical length scale of double-diffusive intrusions. Deep-Sea Res. A 26, 903–913. http://dx.doi.org/10.1016/0198-0149(79)90104-3.

Ruddick, B., Walsh, D., 1995. Observations of the density perturbations which drive thermohaline intrusions. Geophys. Monogr. Ser. 94, 329–334. http://dx.doi.org/10.1029/GM094P0329.

Ruiz-Castillo, E., Sharples, J., Hopkins, J., Woodward, M., 2019. Seasonality in the cross-shelf physical structure of a temperate shelf sea and the implications for nitrate supply. Prog. Oceanogr. 177, 101985.

Schmitt, R.W., Lueck, R.G., Joyce, T.M., 1986. Fine- and microstructure at the edge of a warm-core ring. Deep-Sea Res. A 33 (11–12), 1665–1689. http://dx.doi.org/10.1016/0198-0149(86)90073-7.

Shapiro, S.S., Wilk, M.B., 1965. An Analysis of Variance Test for Normality (Complete Samples). Biometrika 52 (3/4), 591. http://dx.doi.org/10.2307/2333709.

Shcherbina, A.Y., Gregg, M.C., Alford, M.H., Harcourt, R.R., 2010. Three-dimensional structure and temporal evolution of submesoscale thermohaline intrusions in the North Pacific subtropical frontal zone. J. Phys. Oceanogr. 40, 1669–1689. http://dx.doi.org/10.1175/2010JPO4373.1.

da Silveira, I.C.A., Schmidt, A.C.K., Campos, E.J.D., de Godoi, S.S., Ikeda, Y., 2000. A corrente do brasil ao largo da costa leste brasileira. Rev. Bras. Ocean 48, 171–183.

Stech, J.L., Lorenzzetti, J.A., 1992. The response of the South Brazil Bight to the passage of wintertime cold fronts. J. Geophys. Res.: Oceans 97, 9507–9520.

Stern, M.E., 1967. Lateral mixing of water masses. Deep Sea Res. and Oceanographic Abstracts 14, 747–753. http://dx.doi.org/10.1016/S0011-7471(67)80011-1.

Stommel, H., Fedorov, K.N., 2016. Small scale structure in temperature and salinity near timor and mindanao. 19, pp. 306–325. http://dx.doi.org/10.3402/TELLUSA.V19I2.9792.

Suchéras-Marx, B., Escarguel, G., Ferreira, J., Hammer, O., 2019. Statistical confidence intervals for relative abundances and abundance-based ratios: Simple practical solutions for an old overlooked question. Mar. Micropaleontol. 151, 101751. http://dx.doi.org/10.1016/J.MARMICRO.2019.101751.

Thomas, L.N., Tandon, A., Mahadevan, A., 2008. Submesoscale processes and dynamics. Geophys. Monogr. Ser. 177, 17–38. http://dx.doi.org/10.1029/177GM04.

Toole, J.M., Georgi, D.T., 1981. On the dynamics and effects of double-diffusively driven intrusions. Prog. Oceanogr. 10, 123–145. http://dx.doi.org/10.1016/0079-6611(81)90003-3.

Vallat, R., 2018. Pingouin: statistics in Python. J. Open Source Softw. 3 (31), 1026.

Voorhis, A.D., Webb, D.C., Millard, R.C., 1976. Current structure and mixing in the shelf/slope water front south of New England. J. Geophys. Res. 81 (21), 3695–3708. http://dx.doi.org/10.1029/JC081I021P03695.

Walsh, D., Ruddick, B., 2000. Double-diffusive interleaving in the presence of turbulence: The effect of a nonconstant flux ratio. J. Phys. Oceanogr. 30 (9), 2231–2245.

Wang, D.P., Jordi, A., 2011. Surface frontogenesis and thermohaline intrusion in a shelf-break front. Ocean Model. 38, 161–170. http://dx.doi.org/10.1016/J.OCEMOD.2011.02.012.

Welch, C.S., 1981. Mid-level intrusions at the continental shelf edge. J. Geophys. Res. 86, 11013. http://dx.doi.org/10.1029/jc086ic11p11013.

Woods, J.D., Onken, R., Fischer, J., 1986. Thermohaline intrusions created isopycnically at oceanic fronts are inclined to isopycnals. Nature 322, 446–449. http://dx.doi.org/10.1038/322446a0.

You, Y., 2002. A global ocean climatological atlas of the turner angle: Implications for double-diffusion and water-mass structure. Deep-Sea Res. A 49, 2075–2093. http://dx.doi.org/10.1016/S0967-0637(02)00099-7.

Zhurbas, V., Oh, I.S., 2001. Can turbulence suppress double-diffusively driven interleaving completely? J. Phys. Oceanogr. 31 (8), 2251–2254.